Supporting Information

A porous van der Waals single-crystal of aromatic dendrimer exhibiting enhanced thermally activated delayed fluorescence

Shingo Makihara,[a] Sae Nakajima,[a] Hiroyasu Sato,[b] Osamu Oki,[a,c] Takahiro Kondo,[a,c] Yuki Akanuma,[d] Ken Albrecht,*[d] Hiroshi Yamagishi*[,a,c] and Yohei Yamamoto*[,a,c]

[a.] Department of Materials Science, Institute of Pure and Applied Sciences, University of Tsukuba, 1-1-1 Tennodai, Tsukuba, Ibaraki 305-8573, Japan.

[b.] Rigaku Corporation, 12-9-3 Matsubara, Akishima, Tokyo 196-8666, Japan.

[c.] Tsukuba Research Center for Energy Materials Science(TREMS), Hydrogen Boride Research Center (HBRC), Tsukuba Institute for Advanced Research (TIAR), University of Tsukuba, 1-1-1 Tennodai, Tsukuba, Ibaraki 305-8573, Japan.

[d.] Institute for Materials Chemistry and Engineering, Kyushu University, 6-1 Kasuga-koen, Fukuoka 816-8580, Japan.

Materials and Methods.

Unless otherwise noted, all reagents and solvents were used as received from Aldrich Chemical Co. Ltd, Tokyo Chemical Industry Co. Ltd and FUJIFILM Wako Pure Chemical Co. The triazine-carbazole dendrimer was synthesized according to the reported procedures.[32]

Steady-state photoluminescence (PL) spectra were recorded on a JASCO FP8500 spectrofluorometer.

Scanning electron microscopy was performed on a Hitachi model SU-8020 FE-SEM operating at 1 kV. Silicon was used as a substrate.

Powder X-ray diffractometry was conducted at 25 °C on a RIGAKU model Miniflex600 diffractometer with a Cu Kα radiation source (40 kV and 15 mA), equipped with model D/Tex Ultra2-MF high-speed 1D detector.

Variable temperature XRD experiment was performed in a SmartLab diffractometer (Cu Kα, 45 kV, 200 mA, Rigaku) equipped with a variable temperature chamber (TTK 600, Anton Paar) and pixel array Hy-Pix-3000 detector. The sample was placed on a non-diffractive silicon sample plate, and the chamber was repeatedly evacuated using a rotary pump and replaced with nitrogen three times. Finally, the chamber was purged with nitrogen at 1 atm. Measurements were performed in the temperature range of 100 K to 300 K upon cooling and heating with the step of 50 K and 25 K. The temperature increase and decrease rates were 5 K min^{-1}, and measurements were performed after holding the temperature for 5 minutes to ensure uniformity of the sample temperature. Powder XRD data was collected in the range of $2° \leqq 2\theta \leqq 40°$ with a step size and scan speed of 0.02°/step and 20° min^{-1}, respectively.

Continuous rotation 3D electron diffraction data were acquired using the dedicated electron diffractometer JEOL/Rigaku XtaLAB Synergy-ED. Data acquisition was performed at ambient temperature with an electron wavelength of 0.0251 Å (200 kV). The data were processed using CrysAlis^{Pro} for ED, the structure was solved using SHELXT[S1] and the refinement was done by full-matrix least squares on F^2 (SHELXL) [S2], using the Olex2 software package[S3]. Solvent masking was applied during structure refinement. Before solvent masking instruction, structure was refined anisotropically and hydrogen atoms were placed into positions calculated geometrically. Supplementary crystallographic data were deposited at the Cambridge Crystallographic Data Centre (CCDC) under deposition number CCDC-2505553 (G3TAZ) can be obtained free of charge via www.ccdc.cam.ac.uk/data_request.cif .

Optical and fluorescent microscope observations were carried out using an Olympus model BX53 upright microscope. For the fluorescent microscopy, the excitation light with wavelength λ_{ex} = 340–390 nm was used with the long-pass filter (> 410 nm) for the detection of the images.

H_2 adsorption–desorption isotherms up to 12 MPa were obtained at 77 and 298 K using a volumetric BELSORP HP apparatus (MicrotracBEL). The purity of H_2 and He used in experiments was 99.999%. In a N_2-filled glove box, the sample powder was loaded into the measurement cell, capped with a Swagelok SS-8-VCR-2-GR-5M stainless-steel gasket, and assembled with a valve-equipped cell holder. The sealed holder was taken out of the glovebox and then mounted on the instrument without exposure to ambient air. The sample was degassed at room temperature for 12 hours under vacuum. Subsequently, the skeletal volume of the sample at 298 K was determined by dosing He up to 100 kPa. After the skeletal volume measurement, the sample was further degassed at room temperature for 5 hours under vacuum. Afterward, the high-pressure H_2 sorption isotherm was measured up to 12 MPa. The equilibrium time was 500 sec, and the measurement was moved to next point if pressure change was within 0.1% of F.S. pressure.

The PL lifetime measurements were performed using Hamamatsu photonics fluorescence lifetime spectrometer C11367 (Quantaurus-Tau, excitation wavelength of 365nm, and the sample temperature was controlled with an Optistat DN (Oxford Instruments).

The room temperature fluorescence quantum yields were measured by a Hamamatsu Photonics

C9920-02 absolute PL quantum yield measurement system (excitation wavelength: 380 nm).

Variable temperature PL quantum yield (PLQY) measurements were performed by measuring the relative intensity of the PL at several temperatures using a HORIBA JOBIN YVON FluoroMax-4 Spectrometer (excitation wavelength: 365nm, and the sample temperature was controlled with an Optistat DN(Oxford Instruments). The PLQY at various temperatures was calculated by comparison with the room temperature data.

Calculations were performed using TD-DFT at the B3LYP/6-31G(d,p) level based on geometries optimized at the CAM-B3LYP/6-31G(d,p) level. The calculations were performed on a model molecule resembling G3TAZ, in which only a single Cz dendron was retained to reduce the computational cost (Figure S8a). The dihedral angle between the carbazole dendron and the TAZ core was systematically varied, and TD-DFT calculations were performed to determine the S_1 and T_1 energies. All calculations were performed using the Gaussian16 program package [S4].

Supplementary Figures and Tables

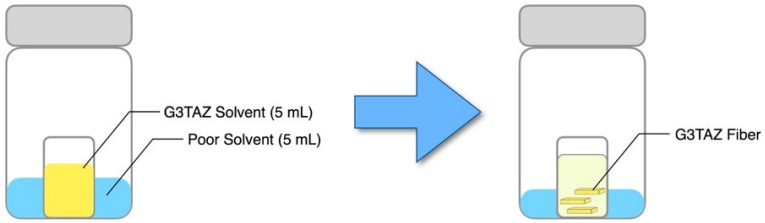

Figure S1. Schematic diagram of vapour diffusion method for the synthesis of crystalline G3TAZ powder.

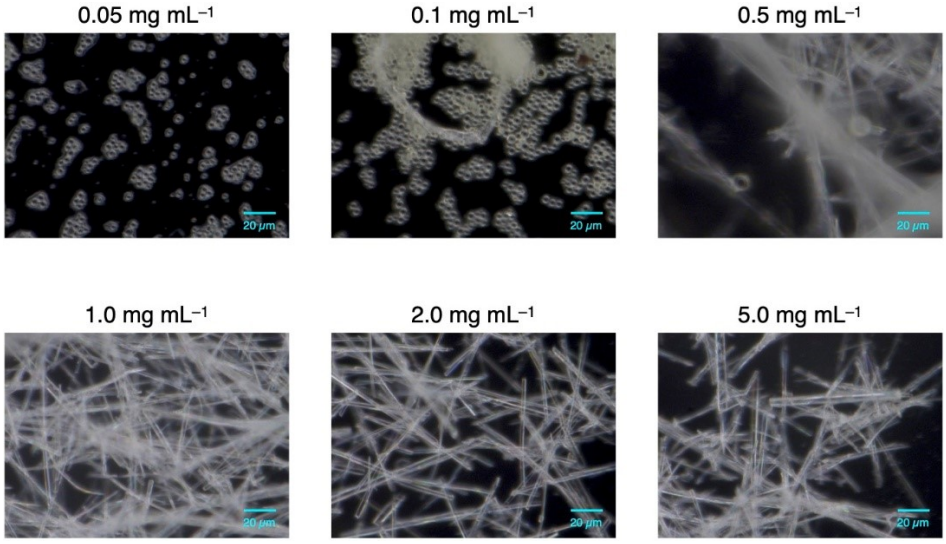

Figure S2. Optical microscopic images of G3TAZ precipitates obtained from solution with a concentration of 0.05–5.0 mg mL^{-1}.

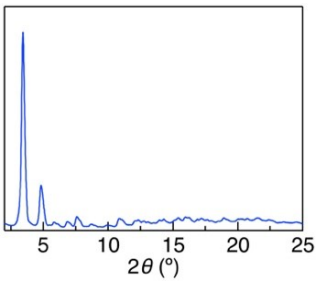

Figure S3. A powder XRD pattern of crystalline powder of G3TAZ.

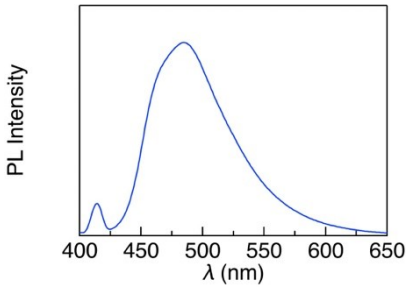

Figure S4. PL spectrum of G3TAZ crystals.

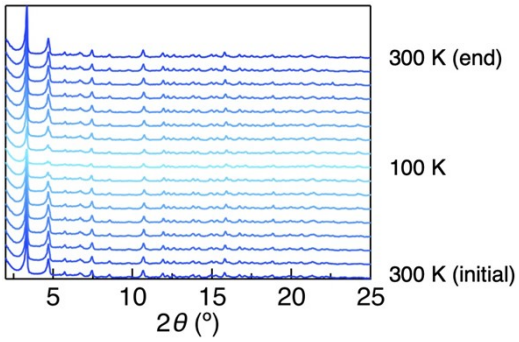

Figure S5. Variable-temperature powder X-ray diffraction profiles of G3TAZ collected during continuous cooling (300–100 K) and heating (100–300 K).

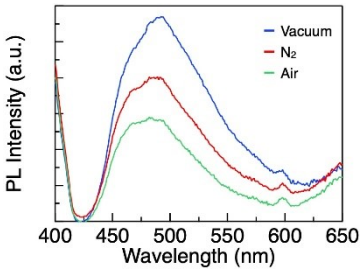

Figure S6. PL spectra of G3TAZ under vacuum (blue), N_2 (red), and air (green) at 300 K.

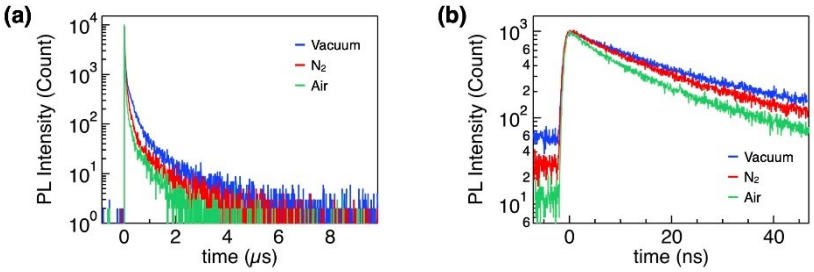

Figure S7. (a,b) PL decay profiles of G3TAZ under vacuum (blue), N_2 (red), and air (green) at 300 K (a), together with their magnified view (b).

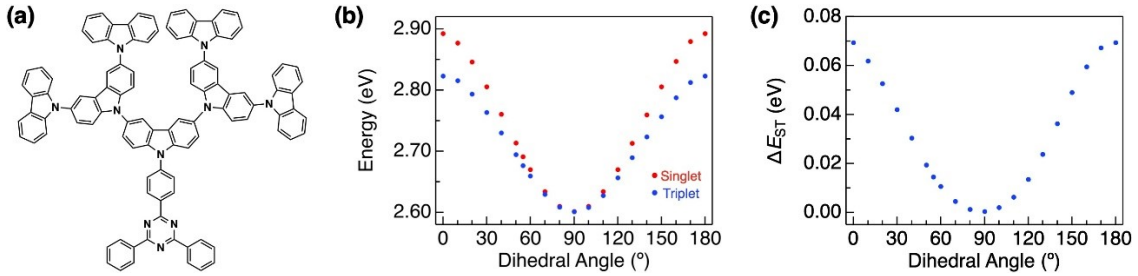

Figure S8. (a) Molecular structure of the model used for the TD-DFT calculations, in which a single Cz dendron of G3TAZ was retained to reduce computational cost. (b) Calculated S_1(red) and T_1 (blue) energies of the model molecule plotted as a function of the dihedral angle between the TAZ core and the Cz dendron. (c) Calculated ΔE_{ST} values of the model molecule as a function of the dihedral angle between the TAZ core and the Cz dendron.

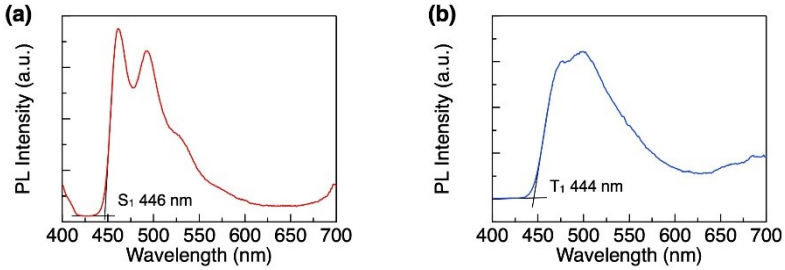

Figure S9. (a) Steady-state PL spectrum of G3TAZ at 77 K. (b) PL spectrum of G3TAZ at 77 K measured with a delay time of 10 ms.

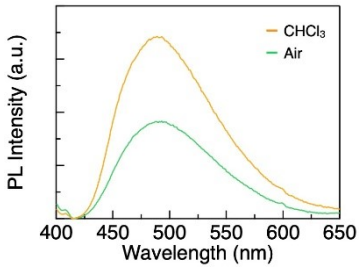

Figure S10. PL spectra of G3TAZ under air (green) and $CHCl_3$ vapor (orange) at 300 K.

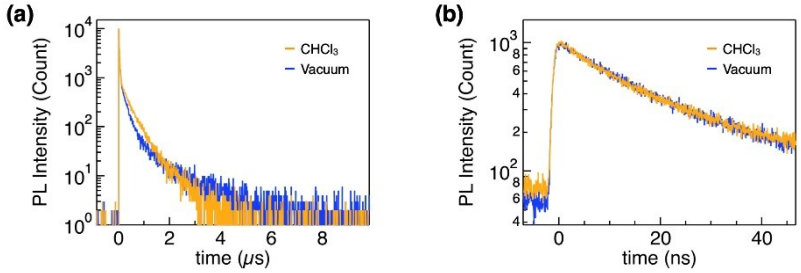

Figure S11. (a,b) PL decay profiles of G3TAZ under vacuum (blue) and $CHCl_3$ vapor (orange) at 300 K.

Table S1. Comparison of molecular weight and BET surface area of representative porous molecular crystals sustained by van der Waals interactions. For reference, porous molecular crystals exhibiting intrinsic porosity are also included.

Material name	Molecular weight	BET surface area ($m^2 g^{-1}$)	Extrinsic or Intrinsic	References
G3TAZ	3778.3	600	Extrinsic	This Work
Py^{open}·MeCN	811.0	597	Extrinsic	S5
$(dipPhO)_8PcCo$	1981.5	970	Extrinsic	21
E_4-1c	961.3	160	Extrinsic	23
VPC-1^{yellow}	1271.5	112	Extrinsic	S6
Boronic ester cage	5629.2	3758	Intrinsic	S7
Porous Organic Cage 2	877.1	533	Intrinsic	S8
Porous Organic Cage 3	1118.5	624	Intrinsic	S8

Table S2. Fluorescence decay parameters of G3TAZ sphere.

G3TAZ Sphere

T (K)	τ_1 (ns)	A_1	τ_2 (ns)	A_2	Sum_{DF}	Sum_{Total}	P_{DF}
77	19.04	661.7	847.7	172.4	15030	88570	0.1697
100	17.93	698.0	1425	94.66	13850	90100	0.1537
125	19.55	674.6	2156	65.58	14240	80820	0.1762
150	18.52	672.4	2270	61.29	14420	79030	0.1825
175	16.65	698.9	3159	56.09	17130	73840	0.2321
200	18.54	692.1	3281	79.63	26110	83860	0.3113
225	17.05	689.8	2958	97.35	28840	85230	0.3384
250	17.86	699.8	2974	114.6	34570	83900	0.4121
275	17.39	701.0	2082	162.1	34680	87810	0.3949
300	16.76	741.3	1849	248.8	32150	78020	0.4122

T : Measured temperature
τ_1 : Fluorescence lifetime of fast fluorescent component
τ_2 : Fluorescence lifetime of delayed fluorescent component
A_1 : Fluorescence intensity at the onset of emission for fast fluorescent component
A_2 : Fluorescence intensity at the onset of emission for delayed fluorescent component
Sum_{DF} : Total number of delayed fluorescent component photons
Sum_{Total} : Total number of photons
P_{DF} : Proportion of delayed fluorescent component

Table S3. Fluorescence decay parameters of G3TAZ crystals.

G3TAZ Crystals

T (K)	τ_1 (ns)	A_1	τ_2 (ns)	A_2	Sum_{DF}	Sum_{Total}	P_{DF}
77	45.66	531.7	9747	48.17	380800	163300	0.1881
100	42.90	826.0	7745	92.81	53380	145300	0.3673
125	34.20	684.5	5433	181.6	85030	148700	0.5719
150	33.28	654.1	4737	302.3	129000	185800	0.6942
175	27.35	554.2	3276	463.8	148400	205600	0.7220
200	24.48	725.2	2281	638.1	147500	204100	0.7226
225	22.02	813.8	1692	737.0	127700	177100	0.7214
250	19.88	668.3	820.4	1047	88470	136800	0.6466
275	19.14	802.0	426.0	1067	46850	95750	0.4893
300	18.89	871.4	260.5	874.8	23780	59920	0.3968

Table S4. Fluorescence decay parameters of G3TAZ cast film.

G3TAZ Cast film

T (K)	τ_1 (ns)	A_1	τ_2 (ns)	A_2	Sum_{DF}	Sum_{Total}	P_{DF}
77	18.10	39.88	898.5	115.2	10660	75320	0.1415
100	17.43	39.84	944.6	115.5	11230	71440	0.1571
125	18.29	40.27	1539	69.37	10950	71980	0.1521
150	19.00	40.19	4221	45.02	17660	71690	0.2463
175	18.42	39.34	3595	55.29	19120	76150	0.2510
200	18.01	41.78	4247	70.14	27640	80070	0.3451
225	18.13	41.02	4137	85.90	32970	85920	0.3837
250	17.78	42.13	3279	106.4	34070	84410	0.4036
275	17.26	42.92	2878	147.8	36230	84500	0.4288
300	17.61	43.54	2092	189.1	35700	82100	0.4348

Table S5. Fluorescence decay parameters of G3TAZ crystals under vacuum, N_2, air, and $CHCl_3$.

Atmosphere	τ_1 (ns)	A_1	τ_2 (ns)	A_2	Sum_{DF}	Sum_{Total}	P_{DF}
Vacuum	18.64	953.1	331.2	850.1	27190	55760	0.4876
N_2	14.17	915.1	331.2	491.7	15710	41220	0.3811
Air	11.84	935.7	344.8	519.0	17230	39880	0.4321
$CHCl_3$	17.06	965.7	392.6	980.1	36730	63300	0.5803

Table S6. Calculated total energies of the singlet and triplet excited states and the resulting ΔE_{ST} values of G3TAZ with dihedral angles of 80° and 55°, representing the conformations in the crystalline and amorphous states, respectively.

	Dihedral angle (°)	Singlet (eV)	Triplet (eV)	ΔE_{ST} (eV)
Crystal	80	2.6099	2.6087	0.0012
Amorphous	55	2.6909	2.6764	0.0145

Supplementary references

S1 G. M. Sheldrick, *Acta Cryst. A*, 2015, **71**, 3–8.

S2 G. M. Sheldrick, *Acta Cryst. C*, 2015, **71**, 3–8.

S3 O. V. Dolomanov, L. J. Bourhis, R. J. Gildea, J. A. K. Howard and H. Puschmann, *J. Appl. Cryst.*, 2009, **42**, 339–341.

S4 Gaussian 16, Revision C.01, M. J. Frisch, G. W. Trucks, H. B. Schlegel, G. E. Scuseria, M. A. Robb, J. R. Cheeseman, G. Scalmani, V. Barone, G. A. Petersson, H. Nakatsuji, X. Li, M. Caricato, A. V. Marenich, J. Bloino, B. G. Janesko, R. Gomperts, B. Mennucci, H. P. Hratchian, J. V. Ortiz, A. F. Izmaylov, J. L. Sonnenberg, D. Williams-Young, F. Ding, F. Lipparini, F. Egidi, J. Goings, B. Peng, A. Petrone, T. Henderson, D. Ranasinghe, V. G. Zakrzewski, J. Gao, N. Rega, G. Zheng, W. Liang, M. Hada, M. Ehara, K. Toyota, R. Fukuda, J. Hasegawa, M. Ishida, T. Nakajima, Y. Honda, O. Kitao, H. Nakai, T. Vreven, K. Throssell, J. A. Montgomery, Jr., J. E. Peralta, F. Ogliaro, M. J. Bearpark, J. J. Heyd, E. N. Brothers, K. N. Kudin, V. N. Staroverov, T. A. Keith, R. Kobayashi, J. Normand, K. Raghavachari, A. P. Rendell, J. C. Burant, S. S. Iyengar, J. Tomasi, M. Cossi, J. M. Millam, M. Klene, C. Adamo, R. Cammi, J. W. Ochterski, R. L. Martin, K. Morokuma, O. Farkas, J. B. Foresman and D. J. Fox, *Gaussian, Inc., Wallingford CT*., 2019.

S5 H. Yamagishi, M. Tsunoda, K. Iwai, K. Hengphasatporn, Y. Shigeta, H. Sato and Y. Yamamoto, *Commun. Chem.*, 2021, **4**, 122.

S6 H. Yamagishi, S. Nakajima, J. Yoo, M. Okazaki, Y. Takeda, S. Minakata, K. Albrecht, K. Yamamoto, I. Badía-Domínguez, M. M. Oliva, M. C. R. Delgado, Y. Ikemoto, H. Sato, K. Imoto, K. Nakagawa, H. Tokoro, S. Ohkoshi and Y. Yamamoto, *Commun. Chem.*, 2020, **3**, 118.

S7 G. Zhang, O. Presly, F. White, I. M. Oppel and M. Mastalerz, *Angew. Chem. Int. Ed.*, 2014, **53**, 1516–1520.

S8 T. Tozawa, J. T. A. Jones, S. I. Swamy, S. Jiang, D. J. Adams, S. Shakespeare, R. Clowes, D. Bradshaw, T. Hasell, S. Y. Chong, C. Tang, S. Thompson, J. Parker, A. Trewin, J. Bacsa, A. M. Z. Slawin, A. Steiner and A. I. Cooper, *Nat. Mater.*, 2009, **8**, 973–978.